ISTITUTO NAZIONALE DI FISICA NUCLEARE

Sezione di Catania

INFN/BE-77/3
12 Dicembre 1977

S. Barbarino, M. Lattuada, F. Riggi, C. Spitaleri and D. Vinciguerra: MOMENTUM DISTRIBUTIONS OF NUCLEONS AND NUCLEAR CLUSTERS FROM QUASI-FREE REACTIONS: A STUDY IN PWIA.

Servizio Documentazione
dei Laboratori Nazionali di Frascati

Istituto Nazionale di Fisica Nucleare
Sezione di Catania

INFN/BE-77/3
12 Dicembre 1977

S. Barbarino(+), M. Lattuada, F. Riggi, C. Spitaleri(+) and D. Vinciguerra(*): MOMENTUM DISTRIBUTIONS OF NUCLEONS AND NUCLEAR CLUSTERS FROM QUASI-FREE REACTIONS: A STUDY IN PWIA(o).

Quasi-free (QF) scattering and reactions have proved to be useful tools in the investigation of the cluster structure of light nuclei(1-12). Plane wave (PW) or distorted wave (DW) impulse approximations are commonly used in the analysis of experimental data extracted from QF measurements. In the framework of the impulse approximation the theoretical triple-differential cross-section can be factorized as follows:

$$\frac{d^3\sigma}{d\,\Omega_1 d\,\Omega_2\, dE_1} = P\,(KF)\,\frac{d\sigma}{d\Omega}\Big|_{free} G^2(P_S) \qquad (1)$$

where P is a factor taking into account absorption effects and clustering probability, (KF) is a kinematical factor, $\frac{d\sigma}{d\Omega}|_{free}$ is the two body "off energy shell" cross section, and $G(\vec{P}_S)$ is given by

$$G(\vec{P}_S) = \int \psi_f^{(1)} \quad \psi_f^{(2)} \chi_{rel} \quad \psi_i^{(0)}\, d\tau \qquad (2)$$

where $\psi_i^{(0)}$, $\psi_f^{(1)}$ $\psi_f^{(2)}$ are the wave functions for the incident and the two outgoing particles, while χ_{rel} describes the relative motion of the two clusters in the nucleus.

Though a DW treatment is able to take into account the presence of absorption and multiple scattering, PWIA has been widely used because, in spite of its simplicity, it predicts reasonably well the shape of the experimental momentum distribution, in regions away from zeros in $G^2(\vec{P}_S)$(13).

When PWIA is used, the factor $G^2(\vec{P}_S)$ in eq. (1) is simply the square of the Fourier transform of the intercluster wave functions χ_{rel}:

$$G(\vec{P}_S) = (2\pi\hbar)^{-3/2} \int e^{-i\vec{P}_S \vec{r}/\hbar}\, \chi_{rel}(\vec{r})\, d\vec{r} \qquad (3)$$

By choosing the $\vec{z}$-axis coincident with the direction of $\vec{P}_S$, the partial-wave expansion of the plane wave becomes

$$e^{-i\vec{K}_S\vec{r}} = \sum_\ell (2\ell+1)(-i)^\ell\, j_\ell(K_S r)\, P_\ell(\cos\theta) \qquad (4)$$

where the j_ℓ's are the Bessel functions and the P_ℓ's the Legendre polynomials of ℓ-th order.

(+) Istituto di Meccanica Razionale e Matematiche Applicate all'Ingegneria dell'Università di Catania.

(*) Istituto di Fisica dell'Università di Catania.

(o) Work supported in part by INFN, CRRN and CSFN/SM.

The intercluster wave function $\chi_{rel}(\vec{r})$ can be expressed as follows:

$$\chi_{rel}(\vec{r}) = \sum_{L,M} R_L(r)\, Y_{LM}(\theta, \phi) \tag{5}$$

where $R_L(r)$ is the radial part and the Y_{LM}'s are the spherical harmonics; the sum is over the L--values which, taking into account the angular momentum and parity conservation laws, are allowed for the intercluster motion.

With the same choice of the reference system and by assuming a single value of L as dominant in the sum, eq. (5), we obtain

$$\chi(\vec{r}) \simeq R(r)\, Y_{LO}(\theta, \phi) \tag{6}$$

By substituting the various factors in eq. (3), and using the properties of the spherical harmonics we can write, for $\ell = L$:

$$G(P_S) = (2\pi\hbar)^{-3/2} \int_{-1}^{1} d(\cos\theta) \int_0^\infty dr \int_0^{2\pi} d\phi\, R(r) Y_{\ell 0}(\theta, \phi) \sum_{\ell'} (2\ell'+1)(-1)^{\ell'} j_{\ell'}(K_S r) \cdot$$

$$\cdot P_{\ell'}(\cos\theta) r^2 = \left[\frac{(2\ell+1)}{2\pi^2 h^3}\right]^{1/2} (-i)^{\ell} \int_0^\infty R(r)\, j_\ell(K_S r) r^2\, dr. \tag{7}$$

As it can be seen from eq. (7), the theoretical momentum distribution $G^2(P_S)$ is determined by the choice of the radial part of the intercluster wave function. The Bessel functions are univocally determined by the angular momentum value, their expression being:

$$j_\ell(K_S r) = \left(-\frac{r}{K_S}\right)^{\ell} \left(\frac{1}{r}\frac{d}{dr}\right)^{\ell} \left[\frac{\sin K_S r}{K_S r}\right]$$

In Fig. 1 are reported the Bessel functions for $\ell = 0, 1$ and 2.

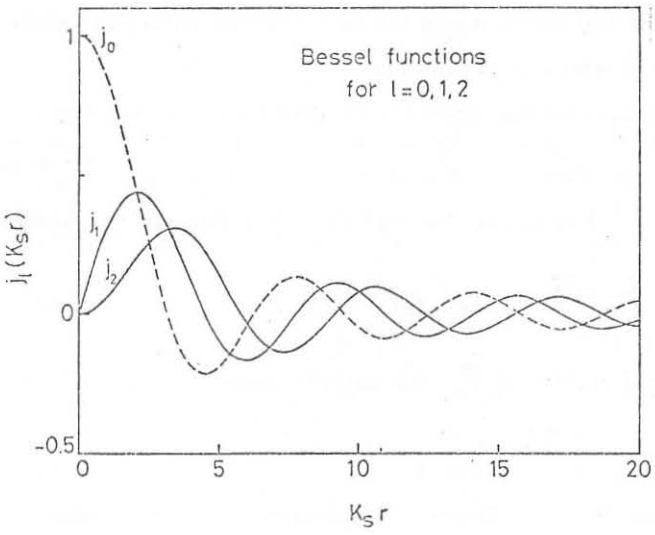

FIG. 1 - Bessel functions reported against $K_S r$, for $\ell = 0, 1, 2$.

As radial part of the intercluster wave function both Hänkel with cut-off and Eckart functions are commonly used.

The Hänkel function with cut-off has the following form

$$H(r) = \begin{cases} 0 & r \leq R_c \\ (2K)^{1/2} \dfrac{e^{-Kr}}{r} & r > R_c \end{cases}$$

where K is the wave number related to the binding energy B of the two clusters by the relationship $K=(2\mu B)^{(1/2)}$, μ being the reduced mass of the system. R_c is a cut-off radius taking into account the absorption effects.

Table I lists the binding energies and the corresponding K-values of the possible two-cluster configurations of the lightest nuclei. Fig. 2 shows the behaviour of the Hänkel function for various K-values, covering the range of interest.

TABLE I - Binding energies and corresponding K values for the two-cluster configurations of the lightest nuclei.

Nucleus	Cluster configuration	B(MeV)	K(fm^{-1})	Nucleus	Cluster configuration	B(MeV)	K(fm^{-1})
^{6}Li	$n+^{5}Li$	5.494	0.468	^{10}B	$n+^{9}B$	8.439	0.603
	$p+^{5}He$	4.655	0.431		$p+^{9}Be$	6.585	0.532
	$d+\alpha$	1.471	0.306		$d+^{8}Be$	6.025	0.679
	$t+^{3}He$	15.790	1.064		$t+^{7}Be$	18.666	1.369
^{7}Li	$n+^{6}Li$	7.252	0.545		$^{3}He+^{7}Li$	17.787	1.337
	$p+^{6}He$	10.006	0.640		$\alpha+^{6}Li$	4.459	0.716
	$d+^{5}He$	9.681	0.813		$n+^{10}B$	11.464	0.706
	$t+\alpha$	2.465	0.450		$p+^{10}Be$	11.237	0.699
^{9}Be	$n+^{8}Be$	1.667	0.266	^{11}B	$d+^{9}Be$	15.822	1.113
	$p+^{8}Li$	16.885	0.847		$t+^{8}Be$	11.230	1.083
	$d+^{7}Li$	16.693	1.115		$^{3}He+^{8}Li$	27.210	1.685
	$t+^{6}Li$	17.687	1.301		$\alpha+^{7}Li$	8.670	1.027
	$^{3}He+^{6}He$	21.185	1.424		$n+^{11}C$	18.722	0.906
	$\alpha+^{5}He$	2.529	0.518		$p+^{11}B$	15.958	0.837
				^{12}C	$d+^{10}B$	25.195	1.417
					$t+^{9}B$	27.360	1.716
					$^{3}He+^{9}Be$	26.286	1.682
					$\alpha+^{8}Be$	7.375	0.970

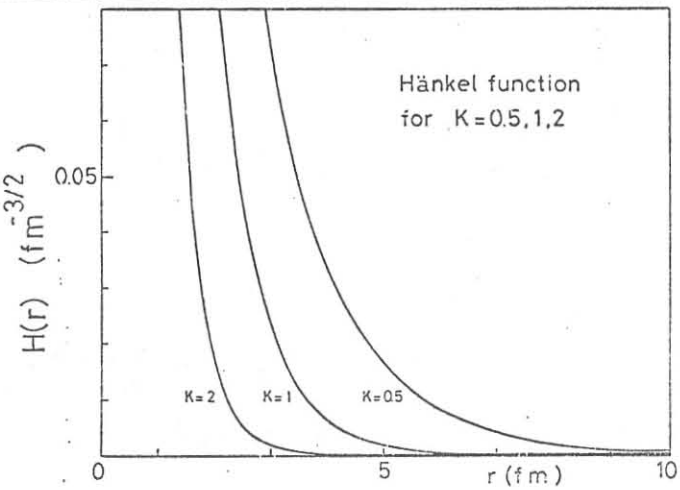

FIG. 2 - Hänkel functions reported against r, for K=0.5, 1, 2.

The Eckart functions, whose general expression is

$$E_n(r) = N_n (1 - e^{-br})^{n+1} \frac{e^{-Kr}}{r}$$

are solutions of the Schrödinger equation with a potential

$$V_n(r) = -\frac{h^2}{2\mu}(n+1)\left[\frac{b^2 + 2Kb}{(e^{br}-1)} - n\frac{b^2}{(e^{br}-1)^2}\right]$$

The parameter b is connected to the root mean square intercluter distance $\sqrt{\langle r^2 \rangle}$ by

$$\langle r^2 \rangle_n = 2 N_n^2 \sum_{\ell=0}^{2n+2} \binom{2n+2}{\ell} \frac{(-1)^\ell}{(\ell b + 2K)^3}$$

where N_n is the normalization constant, given by:

$$N_n = \left[\sum_{\ell=0}^{2n+2} \binom{2n+2}{\ell} \frac{(-1)^\ell}{\ell b + 2K}\right]^{1/2}$$

and K has the same meaning as above.

Fig. 3 and 4 show the shape of the Eckart functions with n=0 and n=1, for different values of b and K.

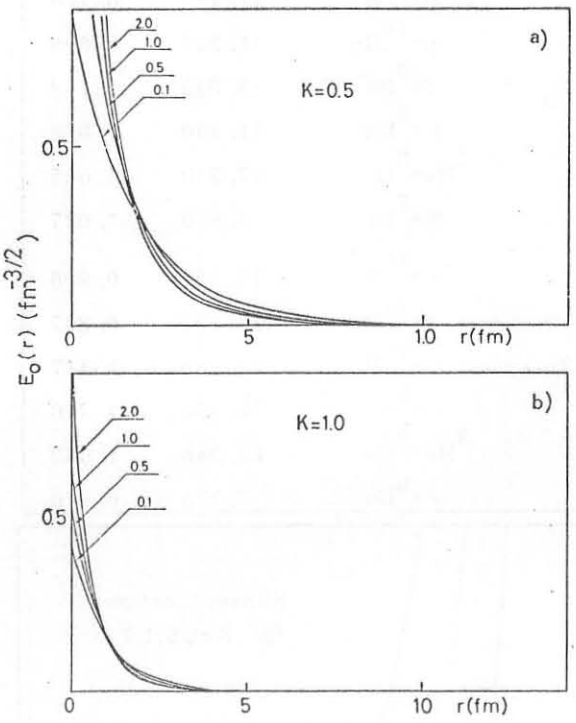

FIG. 3 - Eckart functions with n=0 plotted vs r, with K=0. 5 (3a) and K=1. (3b), for different b-values.

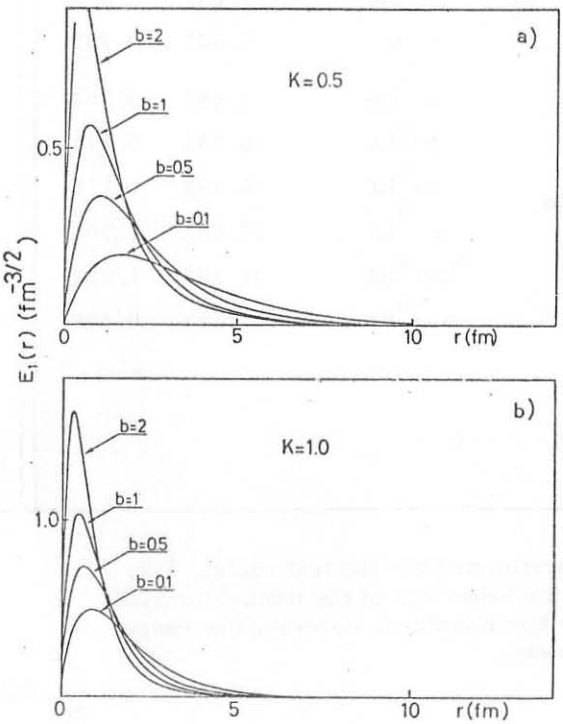

FIG. 4 - Eckart functions with n=1 plotted vs r, with K=0. 5 (4a) and K=1. (4b) for different b-values.

The main difference between Eckart functions with n=0 and $n \geq 1$, lies in their shape at small intercluster distance, the Eckart functions with $n \geq 1$ being similar each other.

Their advantage, with respect to the Hänkel function, is that the asymptotic part, proportional

to e^{-Kr}/r is connected with continuity to the internal part.

The parameter b is not arbitrary, being connected to a meaningful physical quantity as the RMS distance, which in turn can be related, by classical considerations, to the RMS radius of the target nucleus. This connection can be clearly seen from Fig. 5, where the intercluster distance $\sqrt{\langle r^2 \rangle}$ is plotted against b, for the E_o and E_1 functions.

In the present work we have calculated the theoretical momentum distributions $G^2(P_S)$, by numerically integrating eq. (6), using both the Hänkel function with cut-off and the Eckart function with n=1, for different values of ℓ (from 0 to 4) and K(0. 5-1. 0-1. 5 fm^{-1}). Some typical results are reported in Fig. 6; we remark that the various curves, though in arbitrary units are normalized to each other.

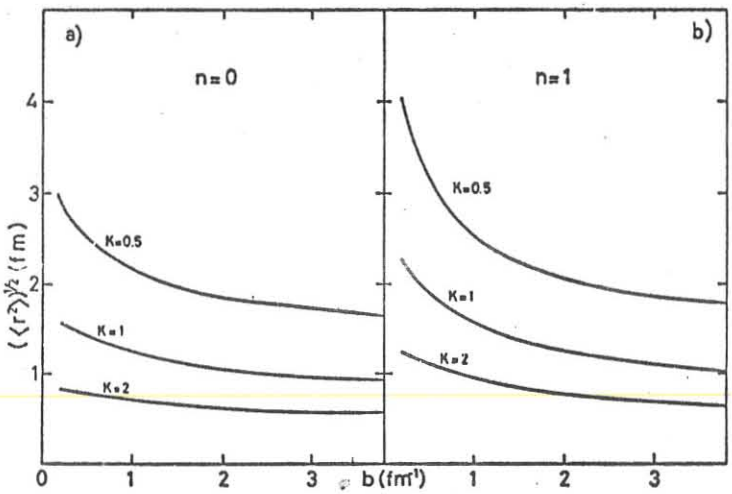

FIG. 5 - The RMS intercluster distance plotted against b, for the Eckart functions with n=0 and n=1(b), for different K-values.

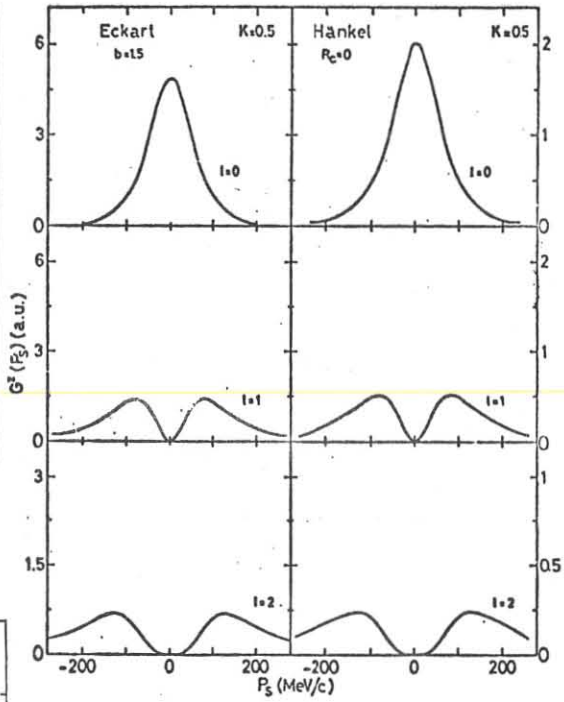

FIG. 6 - Typical momentum distributions as a function of P_S(MeV/c) for ℓ =0, 1, 2. On the left the $G^2(P_S)$ are derived by assuming an intercluster Eckart function with n=1, and b=1. 5. On the right side the momentum distributions are calculated by using a Hänkel function with zero cut-off radius.

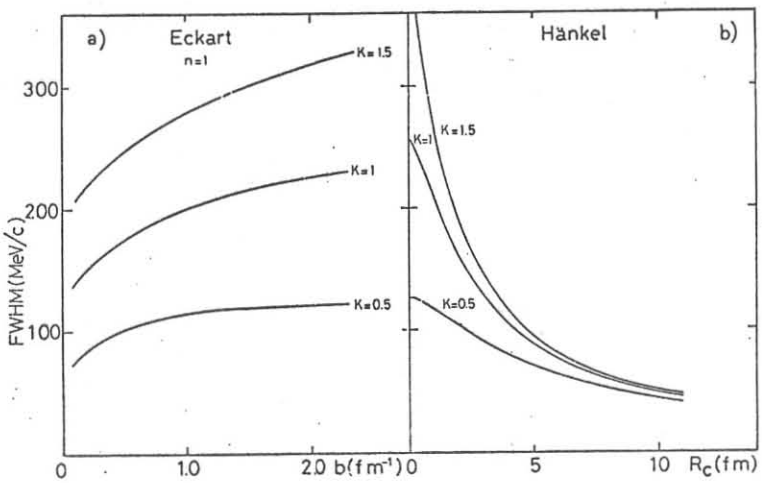

FIG. 7 - Behaviour of the $G^2(P_S)$FWHM, calculated for ℓ =0 both with the Eckart (a) and the Hänkel (b) functions reported against b and R_c respectively.

The FWHM values of the $G^2(P_S)$ with ℓ =0 are also reported in Fig. 7 for the Hänkel and Eckart functions, against R_c and b respectively. Figg. 8-11 show the position of the first maximum in the $G^2(P_S)$ with ℓ =1 to 4 as a function of the same parameters.

The maximum height of $G^2(P_S)$ is reported in Fig. 12 as a function of K and for different ℓ -values, both for Eckart function (with b=1. 5) and Hänkel function (with R_c=0). For ℓ =0 the curves refer to $G^2(P_S=0)$ while for non-zero ℓ values the height of first maximum is drawn.

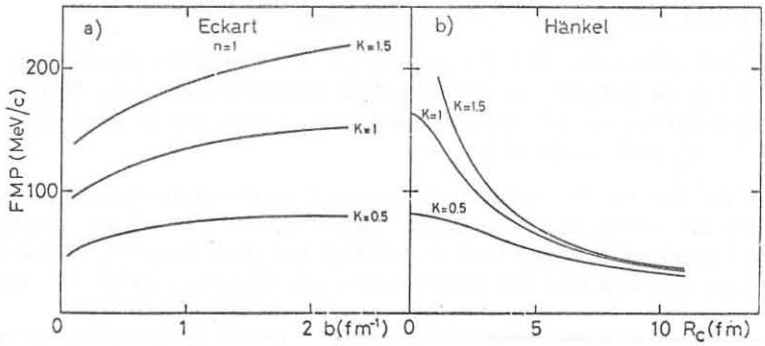

FIG. 8 - First Maximum Positions (FMP) of momentum distributions calculated for ℓ=1, both with the Eckart (a) and the Hänkel (b) functions, reported against b and R_c respectively.

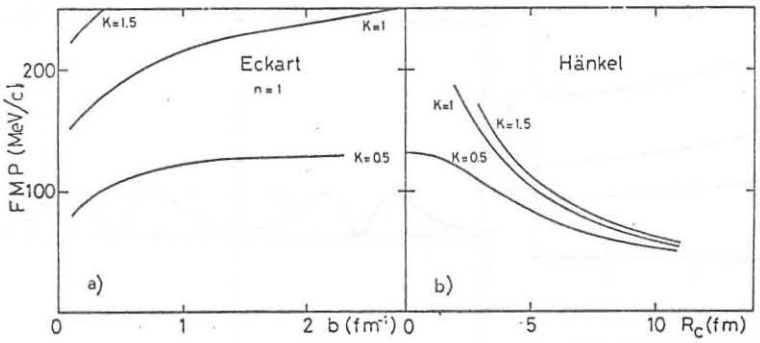

FIG. 9 - As in Fig. 8, for ℓ =2.

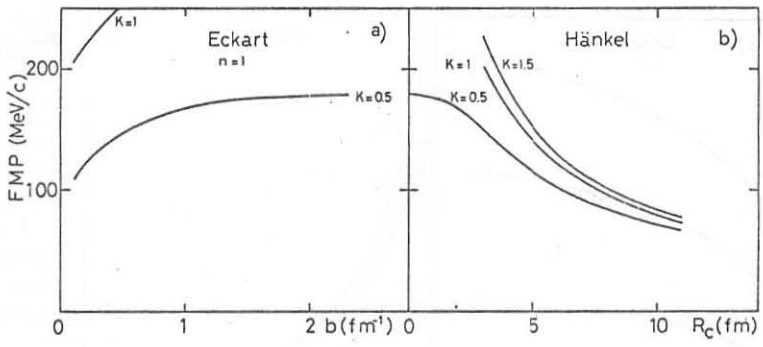

FIG. 10 - As in Fig. 8, for ℓ =3.

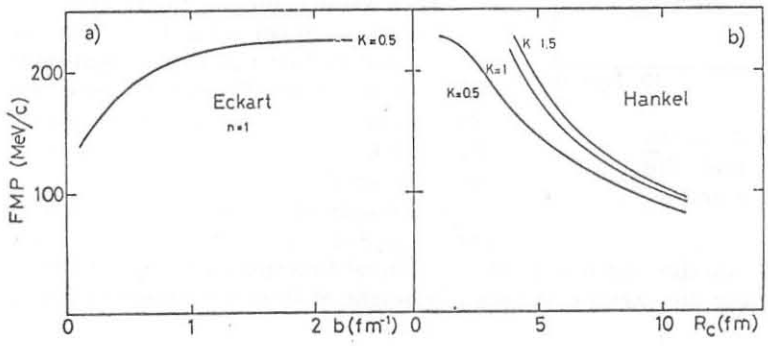

FIG. 11 - As in Fig. 8, for ℓ =4.

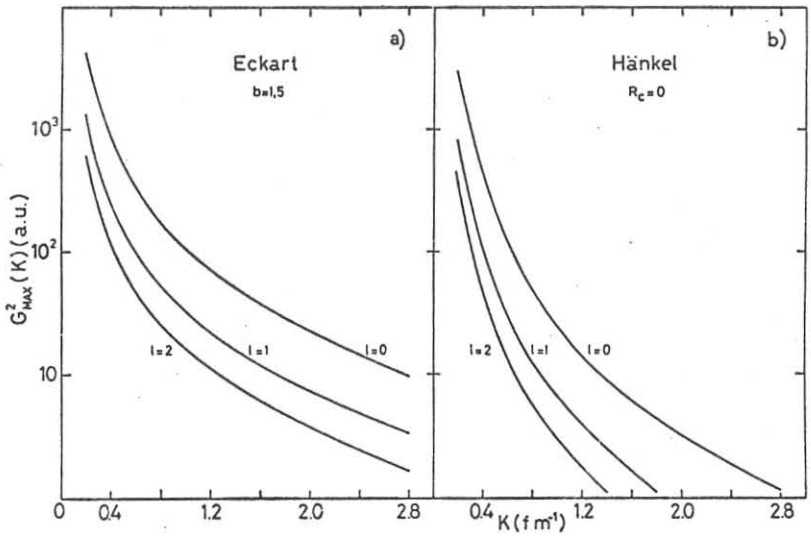

FIG. 12 - First maximum height of $G^2(P_S)$ plotted as a function of K for different ℓ-values, both for the Eckart function with b=1. 5 (a) and the Hänkel function with $R_c=0$ (b).

REFERENCES.

(1) Proc. of the Second Intern. Conf. on Clustering Phenomena in Nuclei, Colleg Park 1975, edited by D. A. Golberg, J. B. Marion and S. J. Wallace (ERDA Technical Information Center, Oak Ridge, Tennessee).

(2) Proc. of the First Intern. Conf. on Clustering Phenomena in Nuclei, Bochum 1969 (International Atomic Agency, Vienna).

(3) Gerhard Jacob and Th. A. J. Maris, Rev. Mod. Phys. 38, 121 (1966); 45, 3 (1973).

(4) M. Riou and Ch. Ruhla, Prog. in Nucl. Phys. 11,195 (1968).

(5) M. Riou, Rev. Mod. Phys. 37, 385 (1965).

(6) Sakae Saito, Jun Hiura and Hajima Tanaka, Prog. of Theor. Phys. 39, 635 (1968).

(7) J. Kasagi, T. Nakagawa, N. Sekine, T. Tohei and H. Ueno, Nuclear Phys. 239A, 233 (1975).

(8) N. Arena, D. Vinciguerra, F. Riggi and C. Spitaleri, Lett. Nuovo Cimento 17, 231 (1976).

(9) N. Arena, D. Vinciguerra, M. Lattuada, F. Riggi and C. Spitaleri, Report INFN/BE-77/2 (1977) and to be published.

(10) M. Lattuada, F. Riggi, S. Barbarino, C. Spitaleri and D. Vinciguerra, Lett. Nuovo Cimento 20, 92 (1977).

(11) D. Miljianic, T. Zabel, R. B. Liebert, G. C. Phillips and V. Valkovic, Nucl. Phys. 215A, 221 (1973).

(12) J. P. Génin, J. Julien, M. Rambaut, C. Samour, A. Palmeri and D. Vinciguerra, Lett. Nuovo Cimento 13, 693 (1975).

(13) P. G. Roos, N. S. Chant, A. A. Cowley, D. A. Goldberg, H. D. Holmgren and R. Woody, Phys. Rev. 15C, 69 (1977).